Fukui Indexes Applied to the Reduced and Nonreduced Species of the Nickel(II) Tetraazadinaphtho[14]annulene Complex and Its Protonated Derivative

Ángel Ríos-Escudero,[†] Juan Costamagna,[†] and Gloria I. Cárdenas-Jirón*[,‡]

Departamento de Química de Materiales, and Laboratorio de Química Teórica, Departamento de Ciencias Químicas, Facultad de Química y Biología, Universidad de Santiago de Chile, Casilla 40, Correo 33, Santiago, Chile

Received: February 18, 2004; In Final Form: June 21, 2004

A first ab initio density functional B3LYP/LACVP theoretical rationalization concerning the determination of the active sites of nickel(II) tetraazadinaphtho[14]annulene (NiN_4CH_3) and its protonated derivative ($NiN_4CH_3H_2$*trans*,*trans*$^{2+}$), when they are submitted to a reduction or an oxidation process, is presented. Condensed Fukui functions (f_k^+ and f_k^-) using the approximations given by *frozen core* (*fc*) and *finite difference* (*fd*) are applied to determine the reductor and oxidant sites. The obtained results of f_k^+ and f_k^- for the nonreduced NiN_4CH_3 and reduced $NiN_4CH_3^-$ species, respectively, predict the nickel atom and the four azomethynic carbon atoms as the most probable active sites, in agreement with experimental results using the pulse radiolysis technique. However, in the protonated structure a different result is found. The nickel atom appears as the unique active site, a reductor site in $NiN_4CH_3H_2$*trans*,*trans*$^{2+}$ and an oxidant site in $NiN_4CH_3H_2$*trans*,*trans*$^{+}$. We also found that both *fc* and *fd* predict the same trend, demonstrating that they are completely valid to be used in the subject of metal complexes and verifying the validity of the partitioning scheme of natural bond orbital used.

1. Introduction

Transition metals, in view of their stereochemical versatility and rich redox reactivity, have an active part in small molecule binding and transport, electron transfer triggering, and fine and selective catalysis due to their structural similarity to active sites of naturally occurring in metalloproteins and metalloenzymes. Thus, the constant interest in the chemistry of the macrocyclic complexes is high.[1−10] The transition metal complexes of tetraaza[14]annulene have attracted much attention for its similarity with porphyrins and corrins in biological systems and their utilities as model compounds in supramolecular systems and material science.[11−14] Among the synthetic metal macrocycles, those containing the tetraazadibenzo[14]annulene system have been studied extensively for the last 3 decades, since the first preparation in 1969 for Jäger[15] is very important stands out against other macrocycles for its synthetic accessibility and high yield.[15−17] Insufficient attention seems to be given to how the ligand structure modifications affect the metal complexes reactivity and in particular its catalytic activity. From this point of view, we have worked with the synthetic macrocycles derived from tetraazadibenzo[14]annulene, that is those containing the tetraazadinaphtho[14]annulene system and its acid−base equilibrium (see Figure 1). These macrocycles are particularly interesting due to its extended π conjugated system which plays an important role in the electro- and photoactivation of carbon dioxide (CO_2).[18−20] In a previous paper,[19] using pulse radiolysis technique on Ni(II) tetraazadinaphtho[14]annulene, we found that the reduction of the metal complex is mainly favored by the ligand. We also did a quantum study of Ni(II) tetraazadinaphtho[14]annulene methyl substituted (NiN_4CH_3) and their four protonated derivatives ($NiN_4CH_3H_2^{2+}$),[20] the isomers *cis*−*cis*, *cis*−*trans*, and *trans*−*trans*, where the positions of the two hydrogens are referred with respect to the naphthalene rings, and the structure with the hydrogens located on the methylenic carbons named as *HinC*. In that study, we calculated the electronic spectra of NiN_4CH_3 and the four structures $NiN_4CH_3H_2^{2+}$ using the ZINDO/CI formalism. Then, we compared the theoretical results with the electronic spectra observed experimentally for NiN_4CH_3 and the protonated compound. The predicted spectrum of NiN_4CH_3 was very similar to that obtained experimentally, and therefore, a good agreement between them was found. In the case of the predicted spectra for the protonated structure, we found that the *trans*−*trans* isomer presents the best agreement with the observed spectrum corresponding to the protonated species.

Fukui function is a local reactivity index that was defined in the density functional theory (DFT) formalism[21] and provides information about the more reactive sites of a molecular system. This index has been applied previously by us in successful way to other transition metals macrocycles.[22−27] The information that Fukui functions provide is relevant when one wishes to know the reactivity of a system in terms of their oxidation sites and of their reduction sites.

Molecular systems such as methyl substituted Ni(II) tetraazadinaphtho[14]annulene (NiN_4CH_3) and their four protonated derivatives ($NiN_4CH_3H_2^{2+}$) have been synthesized for the first time in our laboratory, and there is no information available in the literature reported for these systems. The theoretical study that we present in this work for NiN_4CH_3 and its *trans*−*trans* protonated derivative $NiN_4CH_3H_2$*trans*,*trans*$^{2+}$ constitute the second quantum study that we did for these systems; the first study that we did was performed at a Hartree−Fock semiem-

* To whom correspondence should be addressed. E-mail:gcardena@lauca.usach.cl.

[†] Departamento de Química de Materiales, Facultad de Química y Biología, Universidad de Santiago de Chile

[‡] Laboratorio de Química Teórica, Departamento de Ciencias Químicas, Facultad de Química y Biología, Universidad de Santiago de Chile.

10.1021/jp049250i CCC: $27.50
Published on Web 08/07/2004

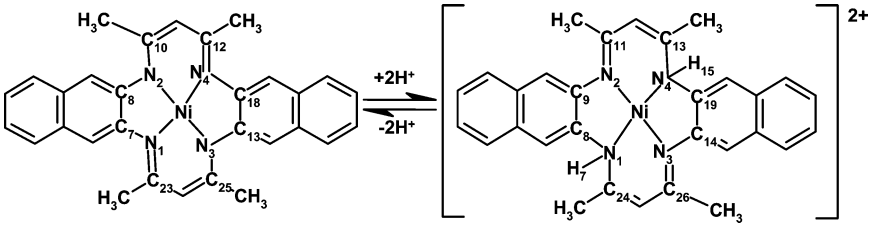

Figure 1. Acid−base equilibrium of NiN_4CH_3 and its protonated derivative $NiN_4CH_3H_2$*trans,trans*$^{2+}$. The numeration of the most important atoms has been included.

pirical level of theory using the ZINDO/CI method.[20] The main contributions of the present work are as follows: (a) It is a study done at the ab initio level of theory using the density functional theory, which is widely proved in the literature to provide good results. (b) It identifies the reduction and oxidation sites of both molecular systems, which for us are relevant to carry out later on one oxidation−reduction study at a quantum chemistry theoretical level that involves these molecules and other substrates such as the carbon dioxide. At an experimental level, we have started to study the reduction of carbon dioxide mediated by these metal transition complexes.[19] The oxidation and reduction sites are determined making use of the condensed Fukui functions. (c) This study allows one to check the validity of the two approximations usually used obtaining condensed Fukui functions, *frozen core* (*fc*) and *finite difference* (*fd*), on large size molecular systems. (d) A full analysis is done studying the effect of the theoretical level used in the geometry optimization on the condensed Fukui functions.

2. Theoretical Background

Density functional theory initially was developed by Hohenberg and Kohn[28] and later by Kohn and Sham[29] and provides a considerable theoretical framework for deriving many quantum chemistry properties. In the DFT context, the electron density $\rho(\vec{r})$ contains information about the molecular system properties and takes a fundamental role in calculating chemical reactivity.[30−32] The Fukui function $f(\vec{r})$, as was proposed by Parr and Yang,[21] is a local reactivity index based in the DFT formalism, and it is defined as

$$f(\vec{r}) \equiv \left(\frac{\delta\mu}{\delta\nu(\vec{r})}\right)_N = \left(\frac{\partial\rho(\vec{r})}{\partial N}\right)_\nu \tag{1}$$

where μ is the electronic chemical potential, $\nu(\vec{r})$ is the external potential, and N corresponds to the total number of electrons. From the reactivity viewpoint, Fukui function is a descriptor that indicates the propensity of the electronic density to deform at a given position to accept or donate electrons.[33] The application of a finite difference approximation to $f(\vec{r})$ condensed to a given atomic region (k)[34] leads to the following operational relations:

$$f_k^+ = \rho_k(N+1) - \rho_k(N) \tag{2}$$

$$f_k^- = \rho_k(N) - \rho_k(N-1) \tag{3}$$

where ρ_k is the electronic population of the atom k evaluated on the neutral species with N electrons, on the anion species with $N + 1$ electrons, and on the cation species with $N - 1$ electrons. f_k^+ is used to analyze the reactive sites for a nucleophilic attack where one electron receiving process occurs in the system, and f_k^- is used to analyze the reactive site for an electrophilic attack where an electron leaving process occurs in the system. f_k^+ (or f_k^-) has a single value for each atom k in the molecule. On the other hand, if we use a molecular orbital viewpoint and a frozen core approximation[35] is applied to f_k, the operational formulas are

$$\begin{aligned} f_k^+ &\approx f_{k,\mathrm{LUMO}} = |\psi^{\alpha,k}{}_{\mathrm{LUMO}}|^2 + |\psi^{\beta,k}{}_{\mathrm{LUMO}}|^2 \\ &= \rho^{\alpha,k}{}_{\mathrm{LUMO}} + \rho^{\beta,k}{}_{\mathrm{LUMO}} \\ &= c^2{}_{\alpha,k,\mathrm{LUMO}} + c^2{}_{\beta,k,\mathrm{LUMO}} \end{aligned} \tag{4}$$

$$\begin{aligned} f_k^- &\approx f_{k,\mathrm{HOMO}} = |\psi^{\alpha,k}{}_{\mathrm{HOMO}}|^2 + |\psi^{\beta,k}{}_{\mathrm{HOMO}}|^2 \\ &= \rho^{\alpha,k}{}_{\mathrm{HOMO}} + \rho^{\beta,k}{}_{\mathrm{HOMO}} \\ &= c^2{}_{\alpha,k,\mathrm{HOMO}} + c^2{}_{\beta,k,\mathrm{HOMO}} \end{aligned} \tag{5}$$

α and β are referred to the electron spin, and HOMO and LUMO are the frontier molecular orbitals, HOMO is the highest occupied and LUMO is the lowest unoccupied. Equations 4 and 5 have the advantage on eqs 2 and 3 that they are easiest to calculate since we only need the wave functions for the frontier molecular orbitals of the ground state. The application of eqs 2 and 3 requires one to perform three theoretical calculations, corresponding to the ground state (N), cationic state ($N - 1$) and anionic state ($N + 1$). Any approximation used for the condensed Fukui function, either *fd* (eqs 2 and 3) or *fc* (eqs 4 and 5) applied on f_k^+ or f_k^-, provides information about the reactive sites in the molecule. In relation to the meaning of a condensed Fukui function, we can say that a maximum value of this gives account of a major change in ρ_k due to a change in the total number of electrons (N). Therefore, the maximum value on f_k^+ (or f_k^-) is associated with the softest site of the molecule and in consequence to the most reactive site. On the contrary, a minimum value of f_k^+ (or f_k^-) implies a minor change in ρ_k, and thus this site corresponds to the hardest site of the molecule and to the less reactive one.[36] It will be recalled that Fukui functions are only valid studying soft−soft interactions between two species. For hard−hard interactions, the charge on each atom dictates where the reaction will occur. In that case, the molecular electrostatic potential would be used which has been proven to be a good descriptor identifying reactive sites.

3. Computational Details

Semiempirical PM3(tm) (tm: transition metal) Hartree−Fock SCF/MO calculations were carried out fully optimizing the ground-state geometry of NiN_4CH_3 and $NiN_4CH_3H_2$*trans,trans*$^{2+}$ and their reduced species $NiN_4CH_3^-$ and $NiN_4CH_3H_2$*trans,trans*$^+$, respectively, which were done without symmetry restrictions. DFT ab initio calculations were also performed with the LACVP basis set where the carbon, nitrogen and hydrogen atoms were calculated at 6-31G basis set level and the nickel atom was calculated with a pseudopotential contained in the LACVP basis set. The obtained PM3(tm) wave functions were also used as

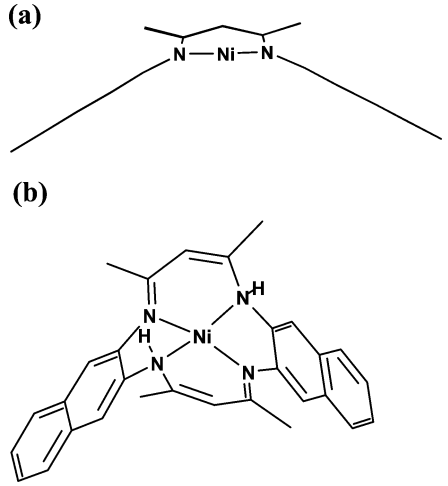

Figure 2. Optimized structures obtained at the B3LYP/LACVP level of theory for NiN_4CH_3 and $NiN_4CH_3H_2$*trans,trans*$^{2+}$.

an initial guess to perform a full geometry optimization at DFT ab initio level using the Becke exchange functional and the LYP correlation functional named as B3LYP. For both optimized geometries (PM3(tm) and B3LYP/LACVP), we did single point calculations at the B3LYP/LACVP level of theory. Therefore, along this paper all of the results to be discussed were obtained at that level. Semiempirical and DFT ab initio calculations were performed with the TITAN package.[37] Both nonreduced structures (NiN_4CH_3 and $NiN_4CH_3H_2$*trans,trans*$^{2+}$) were calculated with a singlet multiplicity; therefore, the calculations performed were carried out with restricted Hartree−Fock (PM3(tm)) and B3LYP (ab initio DFT). Their reduced analogs ($NiN_4CH_3^-$ and $NiN_4CH_3H_2$*trans,trans*$^{+}$) were calculated as a doublet multiplicity; that is the calculations were carried out with the method unrestricted Hartree−Fock (PM3(tm)) and restricted open B3LYP. To determine the condensed Fukui functions using eqs 2 and 3, we have used for the electronic population of the atoms (ρ_k) the partitioning scheme of the electronic density named as natural atomic orbital (NAO) analysis.[38] This partitioning scheme has been used by us with success in previous works for the determination of the condensed Fukui function.[25−27]

4. Results and Discussion

4.1. Structures. As an illustration, Figure 2 schematically shows the optimized structures using the B3LYP/LACVP level of theory of the nonreduced species such as NiN_4CH_3 and $NiN_4CH_3H_2$*trans,trans*$^{2+}$. We have not included the optimized structures for the corresponding reduced species ($NiN_4CH_3^-$ and $NiN_4CH_3H_2$*trans,trans*$^{+}$) because they are very similar to the nonreduced ones. Tables 1 and 2 contain the numerical values for the optimized geometrical parameters associated with the most important atoms of the nonreduced and reduced species. We have defined the most important atoms as the atoms belonging to the annulene system and the metal atom, which have been labeled on each molecule in Figure 1 for the nonreduced species. Note that the same labels used for the nonreduced species are also used for the reduced species.

Table 1, where we included the results for NiN_4CH_3 and $NiN_4CH_3^-$, shows that the ∠NNiN are nearly 180°, suggesting that the NiN_4 center is nearly planar. From the dihedral angles, we found that the deviation of the naphthalene rings with respect to the planarity defined by the NiN_4 center is ∼29° by PM3(tm) and ∼25° by B3LYP/LACVP for NiN_4CH_3. A similar trend is observed for $NiN_4CH_3^-$. On the other hand, the deviation corresponding to the fragments formed by the azomethynic carbons with respect to the planarity of the NiN_4 center is ∼31° by PM3(tm) and ∼29° by B3LYP/LACVP for NiN_4CH_3. The same trend is obtained for $NiN_4CH_3^-$. It is important to note that based in the plane defined by the NiN_4 center, we found that the deviations for the naphthalene rings are inverse with respect to the fragments given by the azomethynic carbons.

Table 2, which includes the results corresponding to $NiN_4CH_3H_2$*trans,trans*$^{2+}$ and $NiN_4CH_3H_2$*trans,trans*$^{+}$, shows a NiN_4 center that is not planar for both levels of theory. It may be seen that for B3LYP/LACVP a pseudotetrahedrical distortion is more evident. The resulting values of dihedral and bending angles for the species appearing in Table 2 are similar to those of the nonprotonated species, but an analysis about the deviation of the different fragments such as the naphthalene rings and

TABLE 1: Optimized Geometric Parameters at the PM3(tm) and B3LYP/LACVP Level of Theory for the NiN_4CH_3 and $NiN_4CH_3^-$ Species[a]

geometrical parameters	PM3(tm)		B3LYP/LACVP	
	NiN_4CH_3	$NiN_4CH_3^-$	NiN_4CH_3	$NiN_4CH_3^-$
		Bond Distances		
N_2Ni	1.855	1.860	1.892	1.923
N_1Ni	1.855	1.854	1.892	1.911
N_4Ni	1.855	1.860	1.893	1.916
N_3Ni	1.855	1.852	1.892	1.924
		Bending Angle		
N_2NiN_3	176.17	178.22	179.01	177.22
N_1NiN_4	176.07	178.88	179.21	179.62
		Dihedral Angle		
$C_{10}N_2NiN_1$	31.20	28.83	28.98	27.73
$C_{23}N_1NiN_2$	31.22	28.96	28.85	27.28
$C_{12}N_4NiN_3$	31.19	26.37	28.87	25.98
$C_{25}N_3NiN_4$	31.16	28.28	28.97	29.10
$C_8N_2NiN_1$	29.37	28.52	24.77	21.38
$C_7N_1NiN_2$	29.32	28.93	24.79	22.15
$C_{18}N_4NiN_3$	29.29	27.83	24.80	22.76
$C_{13}N_3NiN_4$	29.34	27.92	24.75	22.95

[a] Bond distance are in Å and bending and dihedral angles in deg.

TABLE 2: Optimized Geometric Parameters at the PM3(tm) and B3LYP/LACVP level of theory for the $NiN_4CH_3H_2$*trans,trans*$^{2+}$ ($NiN_4CH_3H_2tt^{2+}$) and $NiN_4CH_3H_2$*trans,trans*$^{+}$ ($NiN_4CH_3H_2tt^{+}$) Species[a]

geometrical parameters	PM3(tm)		B3LYP/LACVP	
	NiN_4-$CH_3H_2tt^{2+}$	NiN_4-$CH_3H_2tt^{+}$	NiN_4-$CH_3H_2tt^{2+}$	NiN_4-$CH_3H_2tt^{+}$
		Bond Distance		
N_2Ni	1.852	1.864	1.906	1.950
N_1Ni	1.889	1.890	1.937	2.050
N_4Ni	1.889	1.885	1.936	2.050
N_3Ni	1.852	1.855	1.907	1.950
H_7N_1	1.006	1.005	1.030	1.024
$H_{15}N_4$	1.006	1.004	1.030	1.024
		Bending Angle		
N_2NiN_3	162.07	165.74	158.39	143.94
N_1NiN_4	160.02	164.98	164.01	165.61
		Dihedral Angle		
$C_{11}N_2NiN_1$	31.86	19.88	27.92	26.58
$C_{24}N_1NiN_2$	5.36	3.17	3.17	13.46
$C_{13}N_4NiN_3$	5.38	7.62	3.21	13.35
$C_{26}N_3NiN_4$	31.87	28.40	27.71	26.10
$H_7N_1NiN_2$	65.61	61.45	68.59	75.61
$H_{15}N_4NiN_3$	65.53	64.87	68.59	75.41
$C_9N_2NiN_1$	43.50	49.72	38.30	34.15
$C_8N_1NiN_2$	45.63	49.95	41.16	36.75
$C_{19}N_4NiN_3$	45.60	44.47	41.12	36.88
$C_{14}N_3NiN_4$	43.45	41.78	38.26	34.21

[a] Bond distances are in Å and bending and dihedral angles in deg.

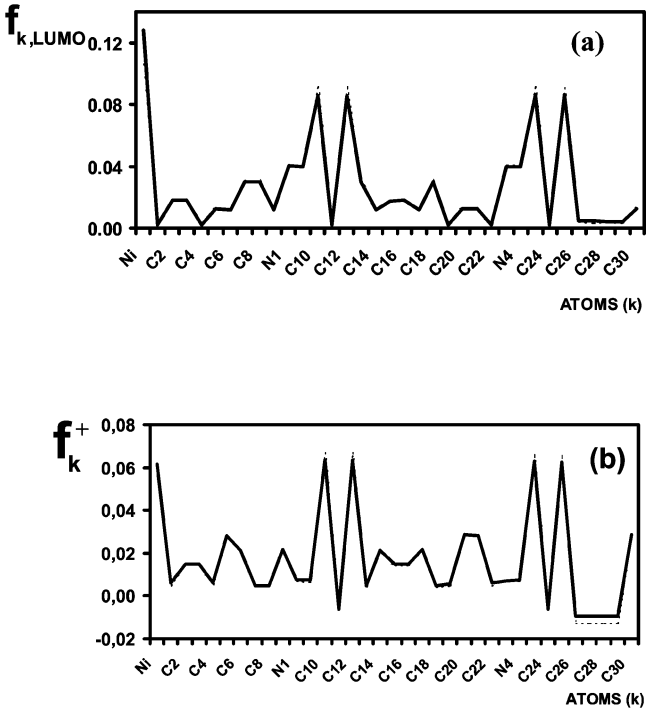

Figure 3. Condensed Fukui indexes for NiN_4CH_3 calculated by the following approximations: (a) frozen core ($f_{k,LUMO}$) and (b) finite difference (f_k^+). Key: (···) PM3(tm) and (−) B3LYP/LACVP optimized geometries.

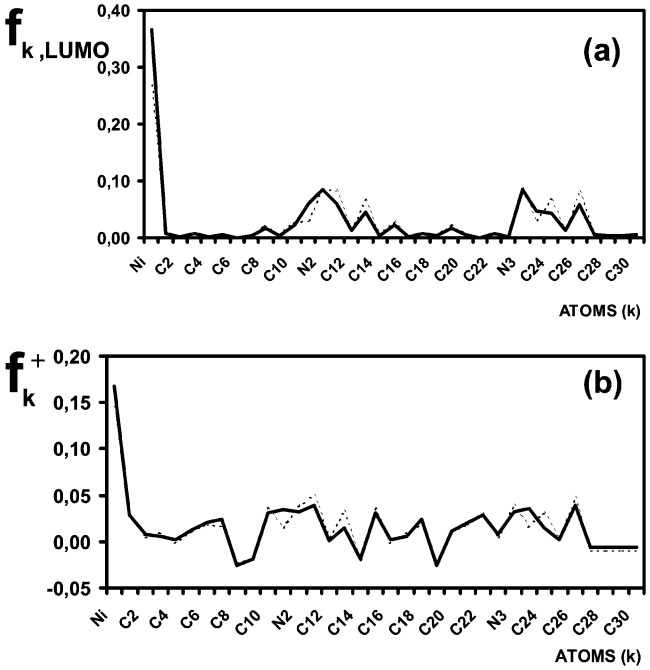

Figure 4. Condensed Fukui indexes for $NiN_4CH_3H_2$*trans,trans*$^{2+}$ calculated by the following approximations: (a) frozen core ($f_{k,LUMO}$) and (b) finite difference (f_k^+). Key: (···) PM3(tm) and (−) B3LYP/LACVP optimized geometries.

azomethynic carbons is more difficult due to the fact that that the NiN_4 center is not planar. The same trend with respect to the direction of the deviation is obtained for both fragments of these species.

4.2. Condensed Fukui Indexes. It is known that in a reduction process of a substrate the species that activates the process should be in its reduced form.[39] It has been reported that in the reduction of CO_2 mediated by nickel macrocycles the active species may correspond to a reduction on the nickel atom, to a reduction on the ligand, or a to cooperative effect between metal and ligand.[7,18,19,40] On the basis of this experimental information, first we will analyze the reduction sites of NiN_4CH_3 and $NiN_4CH_3H_2$*trans,trans*$^{2+}$ in order to know the atomic sites where the electron gain occurs. For this point we will study the f_k^+ condensed Fukui index evaluated on all of the atoms belonging to the macrocycle. Then, we will study the oxidation sites of the reduced species ($NiN_4CH_3^-$ and $NiN_4CH_3H_2$*trans,trans*$^+$) to analyze where the electron loss occurs. The f_k^- condensed Fukui index will be used to determine these sites. We will also discuss the validity of the condensed Fukui functions determined by the approximations of finite difference and frozen core in this kind of Ni(II) tetraazadinaphtho[14]-annulene complexes. Finally, we will analyze the effect that the optimized geometry (PM3(tm) and B3LYP/LACVP) has on the condensed Fukui functions.

4.2.1. f_k^+ Index. Figure 3 shows the results obtained for the f_k^+ Fukui index for NiN_4CH_3 calculated using both optimized geometries obtained at the PM3(tm) and B3LYP/LACVP levels of theory. Figure 3a includes results using the frozen core approximation, and Figure 3b includes the corresponding ones obtained with the finite difference approximation. Figure 4 display the results determined for the f_k^+ Fukui index for the $NiN_4CH_3H_2$*trans,trans*$^{2+}$ nonreduced species using both optimized geometries obtained at the PM3(tm) and B3LYP/LACVP levels. Figure 4a shows the results obtained with the *fc* approximation and Figure 4b includes the corresponding results for the *fd* approximation. As it is shown in Figure 3, parts a and b, the more probable reduction sites correspond to the nickel atom and azomethynic carbon atoms labeled as C_{10}, C_{12}, C_{23}, and C_{25} (see Figure 1). Because the highest value for f_k^+ is obtained for these atoms, we propose these atomic positions as being the preferred reduction sites. We observed that both *fc* and *fd* approximations show the same trend, predicting these atomic sites with the highest values of f_k^+. Note that the same behavior is not obtained for all of the atoms, a slight difference is observed when we compared the f_k^+ values determined with *fc* (Figure 3a) with respect to *fd* (Figure 3b). It is interesting to mention that although these small differences are observed between both approximations, they predict the same reduction sites. These results indicate that a molecular orbital description for a condensed Fukui function such as $f_{k,LUMO}$ defined in eq 4 is completely valid to determine reduction sites along a molecule although this equation only represent information about the frontier of the system. Figure 3 also includes a comparison between f_k^+ obtained using different geometries, semiempirical PM3(tm) and density functional ab initio B3LYP/LACVP. Note that although different geometries are used in both cases the f_k^+ values were obtained at B3LYP/LACVP level of theory. It may be observed in Figure 3, parts a and b, that the results are very similar and do not differ much, indicating that the changes of the optimized geometries between both levels of theory are not significant. In this aspect, we may conclude that, in a study related to Fukui indexes, a semiempirical method such as PM3-(tm) when it is used as restricted Hartree−Fock is completely valid to obtain the optimized geometry of a molecule. Note that a reduced computational time is used for a semiempirical geometry optimization in comparison with that used for a density functional ab initio optimization.

The $NiN_4CH_3H_2$*trans,trans*$^{2+}$ nonreduced species, which corresponds to one of the protonated complexes, was also studied in order to see the effect of the protonation on the reduction sites along the molecule. Figure 4a, which corresponds

to f_k^+ obtained by the *fc* approximation, shows that in this molecule the nickel atom presents the highest value of f_k^+ in comparison with the remaining atoms. It may also be seen in this figure that there is notoriously one unique reduction site that corresponds to the metallic site. The *fd* approximation, as may be seen in Figure 4b, predicts the same result that the *fc* ones; the nickel atom is the reduction site. Now, if we compare the f_k^+ values for the remaining atoms of $NiN_4CH_3H_2$-*trans,trans*$^{2+}$ predicted by *fc* with the ones predicted by *fd*, we found differences between them. *fc* distinguishes the nitrogen atoms (N_2 and N_3) corresponding to the protonated nitrogen atoms as having highest values of f_k^+ than the remain of the ligand. However, *fd* does not see clearly differences between the atoms belonging to the ligand and provides values of f_k^+ very similar along the ligand. In relation to use the PM3(tm) and density functional optimized geometry for $NiN_4CH_3H_2$-*trans,trans*$^{2+}$, we obtained a slight difference for *fc* and *fd*. Using the B3LYP/LACVP optimized geometry, the predicted f_k^+ value for the nickel atom increases with respect to that obtained with the PM3(tm) optimized geometry. The obtained results for f_k^+ by both approximations indicate that the reduction of a metal complex such as NiN_4CH_3 is addressed to the metallic site or to the azomethynic carbon atoms, and it is completely preferred toward the metallic site in $NiN_4CH_3H_2$*trans,trans*$^{2+}$.

It is important to note that the *fd* approximation yields negative values of f_k^+ for some atoms, see Figures 3b and 4b, which represent a small amount of atoms with respect to the whole molecule. The reason for the appearance of negative f_k^+ values is in the partitioning scheme (NAO analysis) used for the electronic density of atoms. The NAO analysis used in this work led in some atoms an electronic population for the anion species $\rho_k(N+1)$ with a lower value than $\rho_k(N)$ for the same atom. When these values are replaced in eq 2, a negative value for f_k^+ is obtained. It is clear that the negative values appear as a result of the partitioning scheme for ρ_k used. However, these values that correspond to carbon atoms belonging to the macrocycle are small in absolute terms (see Figures 3b and 4b). The nonnegative condensed Fukui functions are being widely discussed in the literature[41−49] because it has been shown that different partitioning schemes for the electronic density such as Mulliken population analysis, natural bond orbital analysis, and molecular electrostatic potential derived charges lead in some cases to negative values for the condensed Fukui function. Roy et al.[43,44,46] and Olah et al.[47] have shown that the stockholders charge partitioning technique that corresponds to the Hirshfeld analysis[50] produces nonnegative condensed Fukui function values. Unfortunately, that technique is not available in the quantum chemistry softwares that we hold. Although negative values appear in our study, we found an excellent agreement between the positive values obtained for f_k^+ by finite difference (Figures 3b and 4b) and those obtained by frozen core (Figures 3a and 4a). This agreement demonstrates also the validity of the partitioning scheme of natural atomic orbital analysis in transition metal macrocycles used in the present work.

4.2.2. f_k^- Index. Once we had known the sites where the reduction would occur on NiN_4CH_3 and on $NiN_4CH_3H_2$-*trans,trans*$^{2+}$, then we wanted to investigate from the reduced species ($NiN_4CH_3^-$ and $NiN_4CH_3H_2$*trans,trans*$^+$) where the oxidation would occur, that is which would be the preferred oxidation sites. In Figures 5 and 6 we present the results obtained for the f_k^- Fukui indexes applied to $NiN_4CH_3^-$ and to $NiN_4CH_3H_2$*trans,trans*$^+$, respectively. As in the above section, we

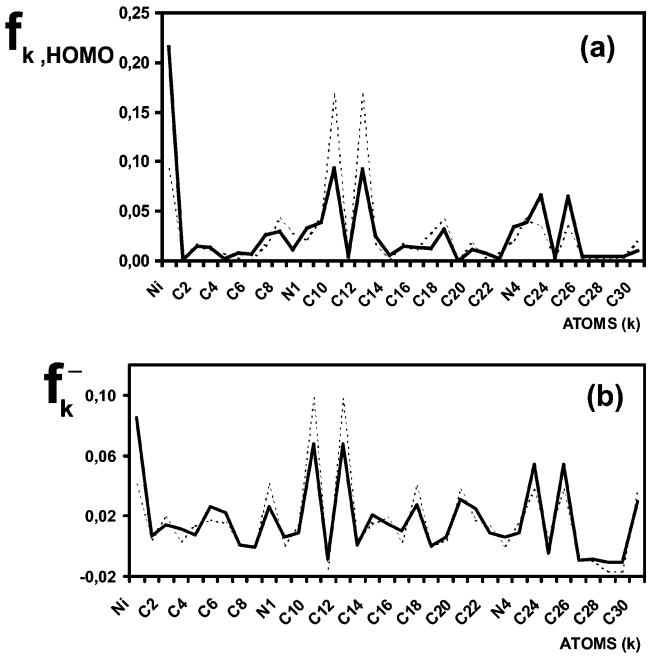

Figure 5. Condensed Fukui indexes for $NiN_4CH_3^-$ calculated by the following approximations: (a) frozen core ($f_{k,HOMO}$) and (b) finite difference (f_k^-). Key: (···) PM3(tm) and (−) B3LYP/LACVP optimized geometries.

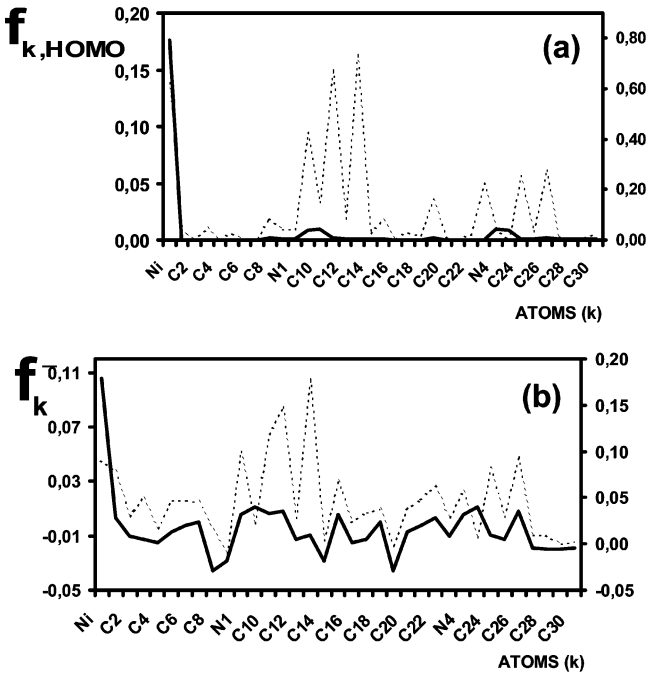

Figure 6. Condensed Fukui indexes for $NiN_4CH_3H_2$*trans,trans*$^+$ calculated by the following approximations: (a) frozen core ($f_{k,HOMO}$) and (b) finite difference (f_k^-). Key: (···) PM3(tm) and (−) B3LYP/LACVP optimized geometries.

included the results using the *fc* approximation (Figure 5a and Figure 6a) and the *fd* approximation (Figure 5b and Figure 6b).

In the case of the no protonated $NiN_4CH_3^-$ species, both *fc* and *fd* approximations predict the same behavior giving to the azomethynic carbon atoms (C_{10}, C_{12}) and not to their symmetric analogues C_{23} and C_{25} as the preferred oxidation sites if a PM3-(tm) optimized geometry is used. Less participation of the nickel atom and of the C_{23} and C_{25} carbon atoms is found. Note that the C_{10} and C_{12} carbon atoms present the highest value of f_k^-. However when a B3LYP/LACVP optimized geometry is used,

the behavior between these atoms is interchanged now predicting the nickel atom as the preferred oxidation site. The carbon atoms named C_{10}, C_{12}, C_{23}, and C_{25} present the lowest f_k^- value. The difference in f_k^- observed between the nickel atom and the carbon atoms mentioned is increased when the *fc* is used. It is known in quantum chemistry that the best theoretical calculation is that performed with the fewest amount of approximations, that is being the most exact. On the basis of this fact, in our study it corresponds to the B3LYP/LACVP optimized geometry, which predicts the nickel atom as the preferred oxidation site by *fc* and by *fd*. However the difference between f_k^- values obtained by different geometries is small and always the same atoms appear as the possible oxidation sites. So, we may conclude until here that there are five positions along the molecule that can act as reductor sites losing one electron. It is important to mention that the same positions were found in the before section as oxidant sites gaining one electron. This means that a reduction (section 4.1) on NiN_4CH_3 or an oxidation (section 4.2) on $NiN_4CH_3^-$ may occur in the same region along the molecule.

The f_k^- values obtained for $NiN_4CH_3H_2$*trans,trans*$^+$ using the *fc* and *fd* approximations shown in Figure 6 indicate that the positions labeled as C_{11} and C_{13} obtained using the PM3(tm) optimized geometry are the preferred oxidation sites, which correspond to the azomethynic carbon atoms. We found that only in the *fc* approximation would one have a agreement between these atoms and the nickel atom that present a similar value for $f_{k,\ \mathrm{HOMO}}$. As occurred for $NiN_4CH_3^-$, an asymmetry was found when a PM3(tm) geometry was used, which means that the azomethynic carbon atoms C_{24} and C_{26}, being symmetric analogues with C_{11} and C_{13}, present lowest values of f_k^-. In both approximations, we found that a B3LYP/LACVP optimized geometry notoriously changed the trend observed on f_k^- with respect to that obtained with PM3(tm) geometry, now predicting the nickel atom as the unique oxidation site. Note that for the B3LYP/LACVP geometry the asymmetry of the azomethynic carbon atoms was not observed. We can conclude that both *fc* and *fd* approximations are coherent, showing the same trend in the preferred reaction sites. Further we observed that. for the reduced species, $NiN_4CH_3^-$ and $NiN_4CH_3H_2$*trans,trans*$^+$, an important effect on the f_k^- condensed Fukui function constitutes the change in the optimized geometry. We also observed that the asymmetry obtained for the azomethynic carbons occurs only for the PM3(tm) geometry.

It is important to mention that although again we obtained negative values of f_k^- for some atoms (see Figures 5b and 6b), its value is negligible in absolute terms with respect to the other atoms, and the agreement of the *fd* results with the *fc* results is very good. The reason why these values appear to be negative is found in the fact that $\rho_k(N-1)$ is obtained with a higher value than $\rho_k(N)$, thus when it is replaced in eq 3 a negative f_k^- value is obtained. As was discussed in section 4.2.1, the obtention of these values is related with the electronic population analysis used in this work corresponding to the NAO analysis. For clarity, we will explain the theoretical basis of the natural atomic orbitals and then we will show the arbitrariness of this population analysis that may be the reason that $\rho_k(N-1) > \rho_k(N)$ in some of our results. Natural orbitals (NOs) are the unique orbitals chosen by the wave function itself as optimal for its own description. Mathematically, the NOs $\{\Theta_i\}$ of a wave function Ψ can be defined as the eigenorbitals of the first-order reduced density operator Γ:[38]

$$\Gamma\Theta_k = p_k\Theta_k (k = 1, 2, ...) \tag{6}$$

here, the eigenvalue p_k is the electronic population (occupancy) of the eigenfunction Θ_k for the molecular electron density operator Γ of Ψ. The density operator is merely the one-electron projection of the full *N*-electron probability distribution for answering questions about one-electron subsystems of the total wave function Ψ. The NAOs incorporate two important physical effects that distinguish them from isolated atom natural orbitals as well as from standard basis orbitals: (a) The spatial diffuseness of NAOs is optimized for the effective atomic charge in the molecular environment (i.e., more contracted if the atom is somewhat cationic, more diffuse if the atom is somewhat anionic); (b) The outer fringes of NAOs incorporate the important nodal features due to steric (Pauli) confinement in the molecular environment. The valence NAOs of the atom therefore properly incorporate both the inner nodes that preserve orthogonality to its own atomic core as well as the outer nodes that preserve orthogonality to filled orbitals on other atoms. A characteristic of NAOs is their strict preservation of mutual orthogonality, as mathematically required for eigenfunctions of any physical Hermitian operator. Each NAO therefore maintains intra-atomic orthogonality to the remaining NAOs on the same atom as well as interatomic orthogonality to those on other atoms.

The NAOs are automatically ordered in importance by occupancy. Consistent with the chemical intuition, only the core and valence-shell NAOs are found to have significant occupancies, compared to the extra-valence Rydberg-type NAOs that complete the span of the basis. The effective dimensionality of the NAO space is therefore reduced to that of the formal *natural minimal basis* (NMB) spanning core and valence-shell NAOs only, whereas the residual *natural Rydberg basis* (NRB) of extra-valence NAOs plays practically no significant role in NAO analysis. This condensation of occupancy into the much smaller set of NMB orbitals, allowing the NRB set be ignored, is one of the most dramatic and characteristic simplifying features of natural analysis. We think that the latter is arbitrary, and it may be the reason why in some atoms we obtained $\rho_k(N-1) > \rho_k(N)$, thus leading to negative values for f_k^-.

In the last few years the Hirshfeld partitioning scheme[50] of the molecular electronic density into fragment densities has been used with success to obtain Fukui indices, and it has been shown that this is the unique partitioning scheme that produces nonnegative Fukui function values.[41−49] The Hirshfeld scheme partitions the molecular ground-state density ($\rho(r)$) into the "stockholder atoms in molecules (AIM)" densities $\{\rho_k^{\mathrm{H}}(r)\}$:[51−55]

$$\rho_k^{\mathrm{H}}(r) \equiv \rho_k^{\mathrm{H}}(\rho;r) \equiv w(r)\rho_k^{\circ}(r) \tag{7}$$

where $\rho_k^{\circ}(r)$ is the isolated atom density. It can also be viewed as modifying the free atom densities in accordance with the common AIM enhancement factor

$$w(r) = \frac{\rho(r)}{\rho^{\circ}(r)}$$

with $\rho^{\circ}(r) = \Sigma_k\rho_k^{\circ}(r)$. The promolecule reference density of the familiar density difference diagrams ($\Delta\rho(r) = \rho(r) - \rho^{\circ}(r)$) consists of the isolated atom densities shifted to the corresponding atomic positions in the molecule. The aspect more important in the Hirshfeld scheme is that it has been shown that this partitioning minimizes the so-called *missing information* (or entropy deficiency) of Kullback and Leibler[56] contained in the AIM densities, relative to that contained in the separated atoms defining the promolecule of the familiar density difference diagrams. Then, the stockholders atoms, which have a theoretical

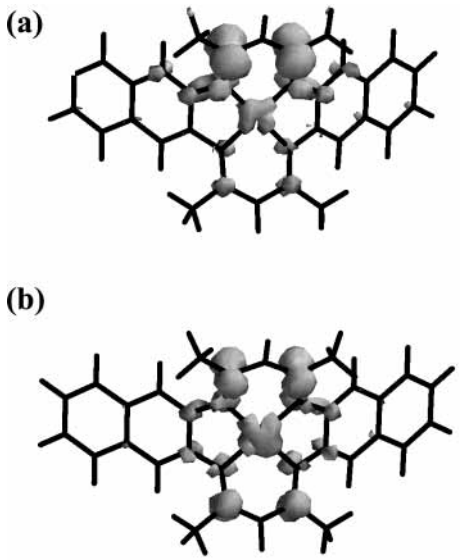

Figure 7. B3LYP/LACVP surfaces of spin density for $NiN_4CH_3^-$ using optimized geometries calculated by (a) PM3(tm) and (b) B3LYP/LACVP.

basis in the information theory, present some advantages: (a) they preserve as much as possible the information contained in the densities of the separated atoms; (b) they exhibit a single cusp at the atomic nucleus, decaying exponentially with increasing distance from it. It has also been shown[53] that only within the Hirshfeld scheme the local measures of information contained in atomic components, e.g., local entropies, of such subsystems equalize at the corresponding global levels of the system as a whole. This equalization of the subsystem information distance densities represents a new, thermodynamic like, entropic criterion of the equilibrium between the molecular subsystems. This condition is complementary to the familiar energetic criterion of the subsystem chemical potential equalization, and represents the missing entropic part of the electronic structure interpretations in chemistry.

4.3. Spin Density. Spin density surfaces were obtained at the B3LYP/LACVP level of theory for $NiN_4CH_3^-$ (Figure 7) and $NiN_4CH_3H_2$*trans,trans*$^+$ (Figure 8) due to that they present an open shell with a doublet multiplicity. Figures 7a and 8a show the results obtained using a PM3(tm) optimized geometry and Figures 7b and 8b display those using a B3LYP/LACVP optimized geometry. In the case of $NiN_4CH_3^-$, we observed an asymmetry in the spin density when the PM3(tm) geometry was used mainly localized on the azomethynic carbons C_{10} and C_{12}. In contrast, when a B3LYP/LACVP geometry was used the spin density is distributed more symmetrically on the azomethynic carbons C_{10}, C_{12}, C_{23} and C_{25}. It is important to note that the same trend was found for the f_k^- condensed Fukui indexes of $NiN_4CH_3^-$ (Figure 5). For $NiN_4CH_3H_2$*trans,trans*$^+$ we also found an asymmetry in the spin density for the calculations using a PM3(tm) geometry localized mainly on C_{11} and C_{13}. However, the spin density obtained with the B3LYP/LACVP geometry changes dramatically leading to a localization highly centered on the nickel atom. These results are in good agreement with those obtained for f_k^- displayed in Figure 6. The asymmetry only observed for the calculations of the reduced species using a PM3(tm) optimized geometry may be understood from the spin contamination found for $NiN_4CH_3^-$ and $NiN_4CH_3H_2$-*trans,trans*$^+$. The spin contamination can be measured from the s^2 value obtained after the SCF procedure. In our case, both molecules present a doublet multiplicity and therefore they should have a value of $s^2 = 0.75$. From the PM3(tm) calculations, we found values of s^2 of 2.69 for $NiN_4CH_3^-$ and of 3.00 for $NiN_4CH_3H_2$*trans,trans*$^+$. Then, these calculations present some degree of spin contamination. Note that the PM3(tm) calculations for these molecules were performed at the unrestricted Hartree−Fock level of theory and the B3LYP/LACVP calculations were performed with a restricted B3LYP level of theory. An unrestricted calculation could modify the spin value producing a spin contamination, but a restricted calculation fixes the spin value and in consequence does not produce a spin contamination. It is important to note that the asymmetry seen for these molecules was not found for the nonreduced species due to that they are closed shell and therefore all the calculations were performed with a restricted method.

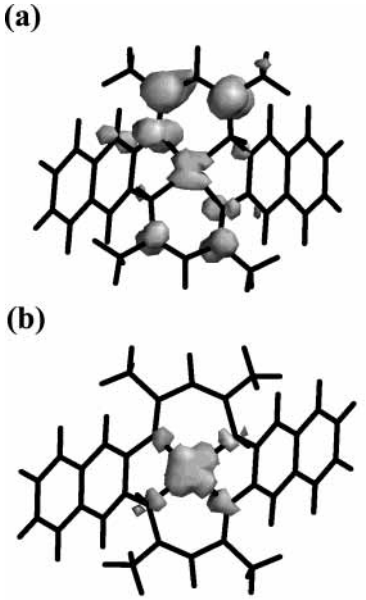

Figure 8. B3LYP/LACVP surfaces of spin density for $NiN_4CH_3H_2$*trans,trans*$^+$ using optimized geometries calculated by (a) PM3(tm) and (b) B3LYP/LACVP.

5. Conclusions

A first density functional theoretical study at the B3LYP/LACVP level of calculation using two different optimized geometries (PM3(tm) and B3LYP/LACVP) to characterize the reduction sites on the nonreduced species, such as NiN_4CH_3 and its protonated analogous $NiN_4CH_3H_2$*trans,trans*$^{2+}$, and the oxidation sites on the reduced species, such as $NiN_4CH_3^-$ and $NiN_4CH_3H_2$*trans,trans*$^+$, was performed. To do that, we determined condensed Fukui indexes calculated by two approximations well established in the literature, *frozen core* and *finite difference*. In general we found a good agreement between the results obtained for the condensed Fukui indexes of the nonreduced species using an optimized geometry with the semiempirical and density functional levels of theory. For the reduced species, some differences for the condensed Fukui indexes are observed when the optimized geometries obtained at the semiempirical and density functional levels of theory are compared. This difference is attributed to the spin contamination obtained when the unrestricted Hartree−Fock method (PM3(tm))was used. In particular, we observed that the nickel atom is favored as the active site (oxidation or reduction) when a B3LYP/LACVP optimized geometry is used. Because *fc* and *fd* predict the same trend obtaining f_k^+ and f_k^-, we conclude that both approximations are completely valid in the field of the metal macrocycles. From this theoretical study, we also conclude that the reduction and oxidation processes on NiN_4-

CH_3 and $NiN_4CH_3^-$, respectively occur on the same atomic positions (Ni and azomethynic C atoms). In contrast, the reduction and oxidation sites for their protonated analogous ($NiN_4CH_3H_2$*trans*,*trans*$^{2+}$ and $NiN_4CH_3H_2$*trans*,*trans*$^{+}$) were found preferably on an unique atomic site, the nickel atom. Although we only have used one partitioning scheme obtaining the electronic population (natural atomic orbital), we verified the validity of our results comparing the two approximations, frozen core and finite difference, which predict the same results.

Acknowledgment. J.C. and G.I.C.-J. express thanks for financial support from Project FONDECYT Lineas Complementarias No. 8010006. G.I.C.-J. thanks the Vicerrectorıa de Investigación y Desarrollo (USACH) for the position of Research Associate. A.R.-E. expresses thanks for a CONICYT Doctorate fellowship.

References and Notes

(1) Truex, T. J.; Holm, R. H *J. Am. Chem. Soc.* **1972**, *94*, 4529.
(2) Baldwin, J. E.; Huff, J. *J. Am. Chem. Soc.* **1973**, *95*, 5757.
(3) Alcock, N. W.; Lin, W.-K.; Jircitano, A.; Mokren, J. D.; Corfield, P. W. R.; Johnson, G.; Novotnak, G.; Cairns, C.; Bush, D. H. *Inorg. Chem.* **1987**, *26*, 440.
(4) Koike, T.; Kimira, E. *J. Am. Chem. Soc.* **1991**, *113*, 8935.
(5) Baldwin, J. E.; Bradley, M. *Chem. Rev.* **1994**, *94*, 715.
(6) Costamagna, J.; Vargas, J.; LaTorre, R.; Alvarado, A.; Mena, G. *Coord. Chem. Rev.* **1992**, *119*, 67.
(7) Costamagna, J.; Ferraudi, G.; Canales, J.; Vargas, J. *Coord. Chem. Rev.* **1996**, *148*, 221.
(8) Trommel, J.; Warncke, K.; Marzilli, L. *J. Am. Chem. Soc.* **2001**, *123*, 3358.
(9) Schrodt, A.; Neubrand, A.; Van Eldik, R. *Inorg. Chem.* **1997**, *36*, 4579.
(10) Ermler, U.; Grabarse, U.; Shima, W.; Goubeaud, S.; Thauer, R. K. *Science* **1997**, *278*, 1457.
(11) Mandon, D.; Giraudon, J. M.; Toupet, L.; Sala-Pala, J.; Gurechais, J. E. *J. Am. Chem. Soc.* **1987**, *109*, 3490.
(12) Hochgesang, P. J.; Bereman, R. D. *Inorg. Chim. Acta* **1989**, *162*, 91.
(13) Cotton, F. A.; Czuchajowska, J. *Polyhedron* **1990**, *9*, 2599.
(14) Caemelbecke, E. V.; Kuntner, W.; Kadish, K. M. *Inorg. Chem.* **1993**, *32*, 438.
(15) Jäger, E. G. *Z. Anorg. Allg. Chem.* **1969**, *364*, 177.
(16) Goedken, V. L.; Pluth, J. J.; Peng, S. M.; Bursten, B. *J. Am. Chem. Soc.* **1976**, *98*, 8014.
(17) Hayes, J. W.; Taylor, C. J.; Hotz, R. P. *J. Chem. Educ.* **1996**, *73*, 991.
(18) Costamagna, J.; Ferraudi, G.; Villagrán, M.; Wolcan, E. *J. Chem. Soc., Dalton Trans.* **2000**, 2631.
(19) Rıos-Escudero, A.; Villagrán, M.; Costamagna, J.; Ferraudi, G. *J. Coord. Chem.* **2003**, *56*, 1233.
(20) Rıos-Escudero, A.; Estiú, G.; Costamagna, J.; Cárdenas-Jirón, G. I. *J. Coord. Chem.* **2003**, *56*, 1257.
(21) Parr, R.; Yang, W. *J. Am. Chem. Soc.* **1984**, *106*, 4049.
(22) Cárdenas-Jirón, G. I. *J. Phys. Chem. A* **2002**, *106*, 3202.
(23) Cárdenas-Jirón, G. I.; Caro, C. A.; Venegas-Yazigi, D.; Zagal, J. H. *J. Mol. Struct. (THEOCHEM)* **2002**, *580*, 193.
(24) Cárdenas-Jirón, G. I.; Venegas-Yazigi, D. A. *J. Phys. Chem. A* **2002**, *106*, 11938.
(25) Cárdenas-Jirón, G. I. *Int. J. Quantum Chem.* **2003**, *91*, 389.
(26) Caro, C. A.; Bedoui, F.; Páez, M. A.; Cárdenas-Jirón, G. I.; Zagal, J. H. *J. Electrochem. Soc.* **2004**, *151*, E32.
(27) Cárdenas-Jirón, G. I.; Parra-Villalobos, E. *J. Phys. Chem. A* **2003**, *107*, 11483.
(28) Hohenberg, P.; Kohn, W. *Phys. Rev.* **1964**, *A136*, 864.
(29) Kohn, W.; Sham, L. *Phys. Rev.* **1965**, *A140*, 1133.
(30) Parr, R.; Pearson, R. *J. Am. Chem. Soc.* **1983**, *105*, 7512.
(31) Koopmans, T. *Physica* **1934**, *1*, 104.
(32) Pearson, R. *Proc. Natl. Acad. Sci. U.S.A.* **1986**, *83*, 8440.
(33) Ayres, P. W.; Parr, R. *J. Am. Chem. Soc.* **2000**, *122*, 2010.
(34) Yang, W.; Mortier, W. *J. Am. Chem. Soc.* **1986**, *108*, 5708.
(35) Chermette, H. *J. Comput. Chem.* **1999**, *20*, 129.
(36) Li, Y.; Evans, J. N. S. *J. Am. Chem. Soc.* **1995**, *11*, 7756.
(37) TITAN 1.0.8, Wavefunction, Inc. and Schrodinger Inc.: 18401 Von Karman Avenue, Suite 370, Irvine, CA 92612 USA.
(38) (a) Weinhold, F.; Landis, C. R. *Chem. Ed.: Res. Practice Eur.* **2001**, *2*, 91. (b) Weinhold, F. *J. Chem. Educ.* **1999**, *76*, 1141. (c) Foster, J. P.; Weinhold, F. *J. Am. Chem. Soc.* **1980**, *102*, 7211. (d) Reed, A. E.; Curtiss, L. A.; Weinhold, F. *Chem. Rev.* **1988**, *88*, 899. (e) Reed, A. E.; Weinhold, F. *J. Chem. Phys.* **1983**, *78*, 4066. (f) Reed, A. E.; Weinstock, R. B.; Weinhold, F. *J. Chem. Phys.* **1985**, *83*, 735.
(39) Fisher, B.; Eisenberg, R. *J. Am. Chem. Soc.* **1980**, *102*, 7363.
(40) (a) Shigeyoshi, S. *J. Am. Chem. Soc.* **1992**, *114*, 2055 (b) Ferraudi, G. *Phthalocyanines: Properties and Applications*; Leznoff, C.; Lever, A. B. P. Eds., VCH: New York, 19XX, Chapter 4. (c) Isaacs, M.; Canales, J. C.; Aguirre, M. J.; Estiú, G.; Caruso, F.; Ferraudi, G.; Costamagna, J. *Inorg. Chim. Acta* **2002**, *339*, 224.
(41) Cruz, J.; Martınez-Aguilera, L. M. R.; Salcedo, R.; Castro, M. *Int. J. Quantum Chem.* **2001**, *85*, 546.
(42) Sivanesan, D.; Subramanian, V.; Unni Nair, B. *J. Mol. Struct. (THEOCHEM)* **2001**, *544*, 123.
(43) Roy, R. K.; Pal, S.; Hirao, K. *J. Chem. Phys.* **1999**, *110*, 8236.
(44) Roy, R. K. *J. Phys. Chem. A* **2003**, *107*, 10428.
(45) De Proft, F.; Martin, J. M. L.; Geerlings, P. *Chem. Phys. Lett.* **1996**, *256*, 400.
(46) Roy, R. K.; Hirao, K.; Pal, S. *J. Chem. Phys.* **2000**, *113*, 1372.
(47) Olah, J.; Van Alsenoy, C.; Sannigrahi, A. B. *J. Phys. Chem. A* **2002**, *106*, 3885.
(48) Misra, G. P.; Sannigrahi, A. B. *J. Mol. Struct. (THEOCHEM)* **1996**, *361*, 63.
(49) Roy, R. K.; Hirao, K.; Krishnamurty, S.; Pal, S. *J. Chem. Phys.* **2001**, *115*, 2901.
(50) Hirshfeld, F. L. *Theor. Chim. Acta (Berlin)* **1977**, *44*, 129.
(51) Nalewajski, R. F. *Phys. Chem. Chem. Phys.* **2002**, *4*, 1710.
(52) Nalewajski, R. F.; Parr, R. G. *Proc. Natl. Acad. Sci. U.S.A.* **2000**, *97*, 8879.
(53) Nalewajski, R. F.; Parr, R. G. *J. Phys. Chem. A* **2001**, *105*, 7391.
(54) Nalewajski, R. F.; Loska, R. *Theor. Chem. Acc.* **2001**, *105*, 374.
(55) Nalewajski, R. F. *J. Phys. Chem. A* **2000**, *104*, 11940.
(56) Kullback, S.; Leibler, R. A. *Ann. Math. Stat.* **1951**, *22*, 79.